University Library

MINERVA ACCESS

A gateway to Melbourne's research publications

Minerva Access is the Institutional Repository of The University of Melbourne

Author/s:
Allen, TG;Bullock, J;Jeangros, Q;Samundsett, C;Wan, Y;Cui, J;Hessler-Wyser, A;De Wolf, S;Javey, A;Cuevas, A

Title:
A Low Resistance Calcium/Reduced Titania Passivated Contact for High Efficiency Crystalline Silicon Solar Cells

Date:
2017-06-21

Citation:
Allen, T. G., Bullock, J., Jeangros, Q., Samundsett, C., Wan, Y., Cui, J., Hessler-Wyser, A., De Wolf, S., Javey, A. & Cuevas, A. (2017). A Low Resistance Calcium/Reduced Titania Passivated Contact for High Efficiency Crystalline Silicon Solar Cells. Advanced Energy Materials, 7 (12), https://doi.org/10.1002/aenm.201602606.

Persistent Link:
https://hdl.handle.net/11343/292411

DOI: 10.1002/ ((please add manuscript number))

Article type: Full Paper

Title: A Low Resistance Calcium / Reduced Titania Passivating Contact for High Efficiency Crystalline Silicon Solar Cells

Authors: Thomas G. Allen, James Bullock, Quentin Jeangros, Christian Samundsett, Yimao Wan, Jie Cui, Aïcha Hessler-Wyser, Stefaan De Wolf, Ali Javey and Andres Cuevas*

T. G. Allen, C. Samundsett, Dr. Y. Wan, Dr. J. Cui, Prof. A. Cuevas

Research School of Engineering

Australian National University

Canberra, Australia, 0200
E-mail: thomas.allen@anu.edu.au

Dr. J. Bullock, Prof. A. Javey

Department of Electrical Engineering and Computer Sciences

University of California

Berkeley, CA 94720, USA

Dr. J. Bullock, Prof. A. Javey

Materials Sciences Division

This is the author manuscript accepted for publication and has undergone full peer review but has not been through the copyediting, typesetting, pagination and proofreading process, which may lead to differences between this version and the Version of Record. Please cite this article as doi: 10.1002/aenm.201602606.

This article is protected by copyright. All rights reserved.

Author Manuscript

Lawrence Berkeley National Laboratory

Berkeley, CA 94720, USA

Dr. Q. Jeangros

Department of Physics

University of Basel

Klingelbergstrasse 82, Basel CH-4056, Switzerland

Dr. Q. Jeangros, Dr. A. Hessler-Wyser

Institute of Micro Engineering

Photovoltaics and Thin-Film Electronic Laboratory

École Polytechnique Fédérale de Lausanne

Maladière 71b, CH-200 Neuchatel, Switzerland

Assoc. Prof. S. De Wolf

KAUST Solar Centre

King Abdullah University of Science and Technology

Thuwal, Saudi Arabia

Keywords: passivated contacts, solar cell, calcium, PERC, TiO_2

Author Manuscript

This article is protected by copyright. All rights reserved.

Abstract: Recent advances in the efficiency of crystalline silicon (c-Si) solar cells have come through the implementation of passivated contacts that simultaneously reduce recombination and resistive losses within the contact structure. In this contribution we demonstrate low resistivity passivated contacts based on reduced titania (TiO_x) contacted with the low work function metal, calcium (Ca). By using Ca as the overlying metal in the contact structure we are able to achieve a reduction in the contact resistivity of TiO_x passivated contacts of up to two orders of magnitude compared to previously reported data on Al / TiO_x contacts, allowing for the application of the Ca / TiO_x contact to n-type c-Si solar cells with partial rear contacts. Implementing this contact structure on the cell level resulted in a power conversion efficiency of 21.8% where the Ca / TiO_x contact comprised only ~6% of the rear surface of the solar cell, an increase of 1.5% absolute compared to a similar device fabricated without the TiO_x interlayer.

1. Introduction

Advances in the efficiency of crystalline silicon (c-Si) photovoltaic (PV) devices above the long-held record efficiency value of 25% have all come from solar cell architectures with passivated contacts fabricated on n-type silicon.[1] The most successful devices to date have a silicon heterojunction (SHJ) cell structure, featuring a thin intrinsic amorphous silicon (a-Si) film that passivates c-Si surface defects, effectively separating the solar cell absorber (c-Si) from the remaining contact materials (doped a-Si, transparent conductive oxides, and metals). This separation of absorber and contact materials avoids extraneous Auger recombination and free carrier absorption losses associated with heavily doped regions, a detrimental feature of diffused junction solar cells. However, the amorphous silicon heterocontact structure necessitates the implementation of large contact

Author Manuscript

This article is protected by copyright. All rights reserved.

fractions due to a relatively high contact resistivity. The trade-off between contact resistivity (ρ_c), contact recombination (J_{0c}), and contact fraction (f_c) is optimised for these devices by minimising J_{0c} and combating the increase in ρ_c by applying the contacts over a large area. However, optical losses arising from parasitic absorption in the doped and intrinsic a-Si layers, as well as the transparent conductive oxide, are a limiting factor in this cell design.[2] Interdigitated back contact structures minimise these losses and have achieved the highest performance for c-Si solar cells,[3] but they still pose challenges for mass production.

Another strategy to achieve high efficiencies is to develop transparent, dopant-free, passivating heterocontacts that minimise ρ_c, thereby allowing the application of the contact structure to devices with low contact fractions, as in the partial rear contact (PRC) architectures commonly known as PERC (passivated emitter and rear cell) and PERL (passivated emitter with rear locally diffused) cells.[4] By minimising ρ_c the constraints on recombination at the contact can be relaxed and the contact can be applied to small areas (f_c < 10%), leaving the remaining surfaces to be passivated with materials that have been utilized by the c-Si PV industry for decades, like silicon nitride (SiN_x) and aluminium oxide (Al_2O_3). These materials are known to effectively eliminate Shockley-Read-Hall (SRH), or defect-assisted, recombination at the silicon surface. Optically this approach can be beneficial, insofar as these materials form non-absorptive and highly reflective optical mirrors when common metals, like Al and Ag, are deposited on top of them. Nevertheless, very few dopant-free electron contacts have been found to date with a sufficiently low ρ_c to be applied to small contact fractions.

Recently, significant progress has been made in the development of directly metallised, dopant-free electron contacts applied to PRC cells fabricated on n-type silicon.[5,6] These device structures have

Author Manuscript

This article is protected by copyright. All rights reserved.

been made possible by applying low work function materials to facilitate low resistivity (ρ_c ~ 2 mΩ.cm^2) Ohmic contacts to undiffused n-type c-Si surfaces. These devices have demonstrated efficiencies of over 20%, but, like the PERC cell architecture, are limited by recombination at the contacts.[7,8] One promising material choice for the formation of a low resistance, dopant-free heterocontact is TiO_2, which has been recently demonstrated to form Ohmic contact on undiffused n-type silicon when applied in conjunction with a low work function Al / LiF overlayer, although no solar cells were fabricated due to the high contact resistivity (ρ_c ~500 mΩ.cm^2).[9] In addition, the work of Yang *et al.* has demonstrated full area Al / TiO_2 electron contacts on the rear side of 19.6% efficient n-type solar cells. With an additional SiO_x interlayer, these devices have shown a remarkable efficiency potential of up to 21.6%, however the application of these contacts is limited to large areas due to their relatively high contact resistivities (300 > ρ_c > 30 mΩ.cm^2) even for TiO_2 thicknesses less than 3 nm.[10,11] In this article we show a reduction of up to two orders of magnitude in the contact resistivity of TiO_2 heterocontacts by replacing the overlying aluminium metal with the low work function metal calcium. In doing so, we demonstrate the compatibility of TiO_2 passivated heterocontacts with n-type c-Si cell designs with partial-area rear contacts, fabricating a first-of-its-kind passivated n-type PRC solar cell with an efficiency of 21.8%.

2. Results and Discussion

2.1. Surface Passivation

Author Manuscript

This article is protected by copyright. All rights reserved.

The passivation of c-Si surface defects by TiO_2 deposited by ALD has been demonstrated previously,[12–14] with surface recombination velocity (SRV; S_{eff}) values below 1 cm/s reported in the literature for TiO_2 films as thick as 15 nm on 10 Ω.cm n-type silicon.[14] The work of Yang *et al.*[11] reports SRV values for thinner TiO_2 films in the range of 56 cm/s to 11 cm/s on 1 Ω.cm n-type substrates for TiO_2 thicknesses between 2.5 nm and 5.5 nm, respectively. (Note that SRV scales with wafer doping in low injection conditions). All studies have reported deleterious effects of temperature on the SRV, even for short annealing times at temperatures over 250 °C, a result of a phase transformation from amorphous to anatase TiO_2.[13,14]

The results of **Figure 1** display the effective minority carrier lifetime of silicon wafers coated with thin ALD TiO_2 layers after a thermal treatment in a forming gas ambient at 250 °C for 5 minutes, following the annealing optimisations in Ref. [11] and [13]. The results show an increase in effective minority carrier lifetime with increasing TiO_2 thickness until saturating at 200 cycles. The SRV values, calculated using the intrinsic lifetime parameterisation of Richter *et al.,*[15] are similar to those reported previously, ranging from approximately 240 cm/s for the thinnest (1.8 nm) to 15 cm/s for the thickest TiO_2 layers (10.5 nm).

2.2. Contact Resistivity

Despite having been a common material for anti-reflection coatings in the c-Si PV industry, and despite its prevalent use in other solar cell devices (*e.g.* dye sensitised and perovskite solar cells), the capacity for TiO_2 to form an electron-selective heterocontact on c-Si has only recently been firmly established.[16] This finding prompted a number of studies into the efficacy of TiO_2 heterojunctions at

Author Manuscript

This article is protected by copyright. All rights reserved.

the device level,[10,17] the most successful implementation of the Al / TiO_2 contact being that of Yang *et al.*, which achieved a power conversion efficiency of 19.8%, increasing to 21.6% with the addition of a SiO_2 interlayer.[11] These devices feature full area TiO_2 contacts on the planarised rear of the solar cells as the contact resistivities of the Al / TiO_2 structures are not compatible with partial rear contact cell designs.

This limitation of the Al / TiO_2 contact is further demonstrated in **Figure 2**a), where the current densities extracted from Cox and Strack test structures are plotted as a function of voltage. The samples were fabricated on 0.9 Ω.cm n-type Si wafers with a heavily phosphorus diffused, aluminium capped rear side to minimise the resistive contribution of the back contact. The undiffused front side feature TiO_2 layers of 3.5 nm and 5.3 nm contacted with Al; the *J-V* data from one control sample without TiO_2 is also shown in the Figure. It can be seen that without the addition of the TiO_2 layer the direct n-type Al / Si contact exhibits a non-Ohmic, rectifying behaviour typical of direct metal / undiffused n-type silicon Schottky contacts. The rectification observed is due to the formation of a large energy barrier for electrons (~0.7 eV) at the Al / Si interface that is empirically ascribed to the Fermi-level pinning phenomenon, in which surface defects limit the metal work function's ability to influence the magnitude of the barrier height at the metal-silicon interface.[18,19] The addition of the 3.5 nm TiO_2 interlayer leads to a reduction of the barrier to electrons compared to the directly metallised case, however the *J-V* data is still representative of a non-Ohmic contact, contrary to the data in [11]. If, however, we restrict the current density in Figure 2a) to a range of ±0.1 A/cm^2 the data appears Ohmic and an approximate extrapolation of ρ_c ~ 150 mΩ.cm^2 can tentatively be made. Such is not the case for the thicker TiO_2 layer where the contact is rectifying at any reasonable current density range at the resolution of this measurement.

Author Manuscript

This article is protected by copyright. All rights reserved.

This interpretation of the *J-V* curves is relevant because the current density at the contacts in a solar cell is proportional to the inverse of the contact fraction (see the inset of Figure 2a)). Very low contact fractions (e.g. f_c = 1%) result in large current densities at an individual point contact, on the order of ~4 A/cm^2 for c-Si devices, while the current density at full area contacts mirrors that of the generation current (minus any quantum efficiency losses) and so is typically less than 0.04 A/cm^2 at the maximum power point. This has a significant impact when interpreting contact resistance data and the applicability of contact structures to devices with large and small area contacts. This would also be a significant consideration when applying these contacts to concentrator cells which are more sensitive to resistive losses and where the generation current density approximately follows the concentration ratio. Additionally, for non-concentrator cells, the Al / TiO_2 contacts shown in Figure 2a) applied to full areas would likely show a signature bending of the Suns-V_{oc} curve typical of rectifying contacts,[20] should a suitably high light intensity value be reached.[21] As such, the 3.5 nm Al / TiO_2 contact resistivity measured in Figure 2a), is certainly suitable for non-concentrator cells with large area contacts, though the value of ρ_c is still higher than the value reported in Ref.[11] but less than a prior report of 250 mΩ.cm^2 for a similarly prepared contact structure.[10] The reason for this difference in reported ρ_c is unclear, however the assertion in Ref.[10], and [11] of Ohmic contact for Al / TiO_2 test structures for TiO_2 thickness up to 5.5 nm may lie in a difference in the range of current densities explored.

The data of Figure 2a) stands in contrast of that of Figure 2b), in which the low work function metal Ca is used as the contact material, instead of Al. As can be seen in Figure 2b), the addition of 3.5 nm of TiO_2 causes a negligible change in contact resistance over the directly Ca-metallised case (ρ_c ~ 5 mΩ.cm^2), while increasing the thickness to 5.3 nm resulted in a non-Ohmic *I-V* response in the as-

Author Manuscript

This article is protected by copyright. All rights reserved.

deposited state. After annealing at 250 °C, a ρ_c of 27 mΩ.cm^2 was measured, increasing to 47 mΩ.cm^2 with a further anneal at 300 °C, a trend of increasing ρ_c also registered for both the directly metallised and thinner TiO_2 samples. Using Al as the metallic overlayer, Yang *et al.* report contact resisitivies of 250 mΩ.cm^2 and 750 mΩ.cm^2 for TiO_2 layers of comparable thickness (3.5 and 5.5 nm, respectively),[10] indicating a remarkable reduction in contact resistivity of 2 orders of magnitude after replacing the Al layer with the low work function metal Ca.

While the ρ_c values measured for the thicker TiO_2 sample are not suitable for the application to devices with partial area contacts, and so are not further explored here, it may be that thicker TiO_2 layers result in lower J_{0c} values after metallisation and so could be applied to larger contact areas. As the current focus is on passivated PRC cells we leave that optimisation for future work.

2.3. PRC Solar Cells

The beneficial effect of the insertion of a TiO_2 passivating interlayer between the rear point contacts and the silicon absorber material in the PRC cell structure (depicted in the cell schematic of **Figure 3**a)) is clearly demonstrated in the *J-V* curves of Figure 3b). Figure 3b) compares the data from the cell reported in Ref. [6] with a similarly fabricated device (this work) featuring both a larger rear contact fraction (6.25% vs 1.26%) and a 3.5 nm TiO_2 passivating interlayer between the Ca metal and the underlying c-Si absorber material. The TiO_2 passivating interlayer has increased the open circuit voltage of the device by nearly 30 mV to 681 mV, an increase in V_{oc} that is reflected in the increase in device efficiency by 1.5% absolute to 21.8%, making this device the most efficient c-Si solar cell with a TiO_2 heterocontact fabricated to date. Remarkably, this increase in efficiency is achieved without an increase in series resistance, but rather a decrease in R_s from 0.8 Ω.cm^2 for the directly metallised

Author Manuscript

This article is protected by copyright. All rights reserved.

cell to below 0.5 Ω.cm^2. This is indicative of a retention of the low contact resistance (ρ_c ~ 5 mΩ.cm^2) despite the addition of the TiO_2 interlayer, as shown in the contact resistance data of Figure 2b), and also due to the application of the contact to a larger area. As the thin TiO_2 interlayer is transparent to IR wavelengths we measure no change in J_{sc}, while the increase in fill factor (*FF*) is a direct consequence of both the lower R_s losses and higher V_{oc}.

Despite the significant increase in V_{oc} measured on the passivated PRC cell, it is apparent from the superposition of the measured efficiency data on to the modelled curves of **Figure S1** that the recombination rate at the Si / TiO_2 interface has increased markedly after the thermal evaporation of the overlying Ca layer. The minority carrier lifetime data of Figure 1 for a 3.5 nm thick TiO_2 passivating layer corresponds to a J_{0c} of approximately 5×10^{-14} A/cm^2. On the cell level the J_{0c} value increases to a value of $J_{0c} < 1\times10^{-11}$ A/cm^2, an increase of ~2.5 orders of magnitude. Improving the J_{0c} value, either by a different choice of passivating interlayer, or through the insertion of a thin SiO_2 layer, as per Ref. [11], remains critical to achieving device efficiencies competitive with other passivated contact technologies. Another pathway to higher efficiencies may lie in replacing the Ca layer with a less reactive, low work function material. Nevertheless, the devices presented here represent the first n-type c-Si passivated partial rear contact cells and conclusively demonstrate the benefits of such a device architecture.

2.4. Structure and Composition of the Contact

The composition and stoichiometry of the as-deposited TiO_2 ALD layer has been analysed by XPS. The survey scan (not shown) identified peaks in the spectra associated with Ti, and O elemental species as well as carbon contamination from the organic precursor. The Ti 2p core level spectrum,

Author Manuscript

This article is protected by copyright. All rights reserved.

displayed in **Figure 4**, shows the peak positions of the Ti $2p_{1/2}$ (464.5 eV) and Ti $2p_{3/2}$ (458.7 eV) electron spin orbitals, a spin-orbit splitting of 5.8 eV, characteristic of Ti^{4+} species in TiO_2,[22–24] evidience of a stoichiometric as-deposited TiO_2 layer. The O1s spectrum (inset) has been deconvolved into two singlets: a main peak at 530 eV with a small shoulder at 531.6 eV. The main peak (O1s A) is representative of the direct oxygen (O^{2-}) bonding to the Ti^{4+} in stoichiometric TiO_2, while the shoulder (Os1 B) is often attributed to absorbed atmospheric oxygen (O_2) or hydroxyl (O-H) bonding from atmospheric H_2O, or perhaps residual H_2O from the deposition process.[25-28] Comparing the relative atomic percentages of the O and Ti components of the TiO_x layer indicates a near stoichiometric atomic ratio of $x \sim 2.09$. Excluding the oxygen content from the O1s B shoulder in the O1s spectrum reduces the atomic ratio to $x = 2$.

STEM HAADF imaging coupled to EDX or EELS has been performed to further investigate the contact structure and composition after Al / Ca evaporation. The STEM HAADF micrograph and corresponding Al, Ca, O, Ti and Si EDX maps shown in **Figure 5**a) highlight the uniform titanium oxide layer separating the silicon absorber from the overlying Al / Ca contact metals. The EDX data also shows an intermixing of the Al / Ca layers and the accumulation of O in the Ca layer close to the Ca / TiO_x interface. While the surface of the Ca is likely to have oxidised slightly during the transfer from the FIB to the TEM, this effect should give rise to a more uniform O EDX signal at the position of the Ca layer than that observed in Figure 5a). Therefore, it is likely that the fluctuation in the O signal observed in the EDX image of Figure 5a) arises from interactions between the TiO_x and the Ca layers.

Also observable in Figure 5a) is the apparent diffusion of Ca through the TiO_x layer. This is supported by the EEL spectra (Figure 5c)) recorded across the high-resolution STEM image shown in Figure 5b) which detect Ca in the TiO_x layer. The EELS data also highlights some intermixing between Si, Ca and

Author Manuscript

This article is protected by copyright. All rights reserved.

Ti over ~2 nm (arrowheads in Figure 5c)), an observation that might be influenced by FIB-induced damage or the sample tilt. In agreement with EDX results, the EELS data demonstrates that O is present mainly on the Ca side of interface with the TiO_x layer (shown by the arrow in Figure 5c)). Higher energy resolution EEL spectra of the Ti $L_{2,3}$ and O K edges of Ca / TiO_x and Al / TiO_x contact structures are shown in Figure 5d). In contrast to the stoichiometric TiO_2 composition inferred from the XPS data after deposition, an estimation of the Ti to O atomic ratio using EELS partial scattering cross sections yields a composition closer to TiO, irrespective of whether it is in contact with Ca or Al. The quantification procedure was performed using the software Digital Micrograph (Gatan, Pleasanton, USA) and involved the computation of a power law background ($A E^{-r}$, where E is the energy-loss in eV, A and r fitting parameters) in the range 410 to 430 eV (for the Ti $L_{2,3}$ edges) and 513 to 528 eV (for the O K edge), the extrapolation of this background and its subtraction to the EELS signal in the range 456-476 eV and 532-572 eV, respectively, to yield the integrated Ti and O core loss intensities. These intensities are then related to elemental ratios using scattering cross sections (which have an accuracy on the order of 10%). It should be mentioned that while the shape of the Ti $L_{2,3}$ edges is indicative of its oxidation state, the amorphous nature of the TiO_x layer (as demonstrated in Figure 5b)) complicates any fine structure fingerprinting procedure. Indeed, the lack of crystallinity prevents the splitting of the L_2 and L_3 edges into further peaks irrespective of the oxidation state, meaning that the fine structure of cubic (and presumably amorphous) TiO appears similar to that of amorphous TiO_2.[29,30] Overall, these results indicate that the Ca (and Al) uniformly reduces the neighbouring TiO_2 layer to a stoichiometry closer to TiO_x, where x ~ 1. This, in part, can explain the build-up in oxygen at the Ca / TiO_x interface observed by EDX and EELS in Figure 5:

Author Manuscript

This article is protected by copyright. All rights reserved.

evidence of the spontaneous migration of oxygen from the as-deposited stoichiometric TiO_2 to the overlying Ca layer.

The reaction kinetics of metal / TiO_2 interfaces have been studied by Fu and Wagner,[31] who found the interfacial reactivity (in this instance, the extent of O^{2-} transfer at the interface) to be dependent on the overlying metal work function. They demonstrated by XPS analysis on thin metal overlayers (~6 Å) the reduction at room temperature of TiO_2 by Al, the lowest work function metal studied, which is in agreement with the EELS data shown in Figure 5d) for the case of a direct contact between TiO_2 and Al. Since the work function of Ca (ϕ ~ 2.9 eV) is considerably lower than that of Al (ϕ ~ 4.2 eV) it follows that the reduction of the TiO_2 would occur, and likely to a greater degree. Furthermore, the preceding interpretation of the EELS data suggesting the reduction of the TiO_2 to TiO is supported by the XPS data of Demri *et al.*[32] in which the interface of crystalline TiO_2 and Ca was investigated. The authors also report on the formation on TiO and CaO layers due to the transfer of oxygen from the TiO_2 to the overlying thermally evaporated Ca layer. The reduction of TiO_2 by an overlying metal layer has also been proposed elsewhere as being critical to contact formation in TiO_x electron selective heterojunctions on c-Si, where the reduction in the titanium oxide is proposed to enhance electron transport through the layer by increasing its conductivity,[33] and either improving the band alignment with the silicon surface or reducing the barrier height at the metal / TiO_x interface.[11,34]

While there is a growing body evidence, including that presented here, suggesting a reduction in the TiO_x layer is one factor in enabling electron contact formation with c-Si, the presence of other effects complicates the analysis in this case. Of particular consideration is the difference in the work function of the contact metal used here, as opposed to other TiO_2 / c-Si electron contacts reported

Author Manuscript

This article is protected by copyright. All rights reserved.

in the literature. Given the similarities in EEL spectra in Figure 5d), it is apparent that the low work function of the Ca layer is one of the main drivers behind the reduction in ρ_c for the Ca / TiO_x, compared to the Al / TiO_x, contact. Additionally, the apparent reduction of the TiO_2 passivating layer implies an oxidation of the overlying, and interdiffused, Ca layer (and Al and Ti layers in Ref. [11] and [34]). This may explain the sensitivity of ρ_c to TiO_2 thickness, though some presence of CaO_x is evidently tolerable in forming low contact resistivities. It is likely that both the change in stoichiometry of the TiO_x layer and possibly the diffusion of Ca into the TiO_x have had an impact on the passivation of the contact structure, explaining the large discrepancy in S_{eff} prior to metallisation and the implied J_0 at the contact from Figure S1b). However, the extent to which each of the factors identified above are influencing the J_{0c} and ρ_c (and hence the device performance) is difficult to distinguish from the data.

3. Conclusion

The use of the low work function metal calcium has enabled the fabrication of a low resistance, dopant-free TiO_x passivated electron heterocontact to undiffused n-type c-Si substrates. The contact resistivity of the Ca / TiO_x / c-Si contact (~5 mΩ.cm^2) represents a reduction in ρ_c by two orders of magnitude over previously reported data for TiO_x / c-Si heterocontacts. Analytical transmission electron microscopy of the contact has revealed a reduction of TiO_2 layer by the overlying Ca metal that is likely to have assisted in the lowering of the contact resistivity but compromised the passivation of c-Si surface defects at the TiO_x / Si interface. Nevertheless, the extreme reduction in contact resistance compared to other TiO_x-based heterocontacts reported in the literature, as well as the reduction in recombination at the TiO_x / Si interface, has enabled the fabrication of a first-of-

Author Manuscript

This article is protected by copyright. All rights reserved.

its-kind passivated partial rear contact n-type silicon solar cell with an efficiency of 21.8%, making this device the most efficient c-Si solar cell with a TiO_x heterocontact fabricated to date.

4. Experimental Section

The TiO_2 layers in this study were deposited by atomic layer deposition (ALD, Beneq TFS 200) by sequential exposure of titanium isopropoxide (TTIP) and de-ionised water. The TTIP was heated to a temperature of 40 °C, while the deposition chamber was held at 230 °C. Symmetrically passivated lifetime samples were prepared on planar saw-damage etched, RCA cleaned, silicon substrates that were dipped in dilute HF prior to further processing. The effective lifetime (τ_{eff}) of the passivated samples was measured as a function of minority carrier injection level (Δn) on a Sinton Instruments WCT120 photoconductance tester operating in quasi-steady-state and transient modes. X-ray photoelectron spectroscopy (XPS, Thermo Scientific ESCALAB 250Xi) survey and core level scans were performed on the TiO_2 layers with a monochromatic Al Kα (1486.68 eV) X-ray source at a vacuum pressure of $< 2\times10^{-9}$ mbar. The stoichiometry of the as-deposited TiO_2 was determined from the atomic percentage calculations taken from the XPS data after subtraction of the Shirley background using the software Advantage (Thermo Scientific, USA).

Thin, ~30 nm, layers of Ca were thermally evaporated vacuum pressures $< 1\times10^{-6}$ Torr from a solid source in a glovebox-integrated metal evaporator. An initial ~150 nm capping layer of Al was sequentially evaporated in the same chamber without breaking vacuum. A further ~150 nm of Al was subsequently evaporated after breaking vacuum to thicken the capping layer. Contact resistance measurements were performed using Cox and Strack (with a rear side Al / n^+ contact) and transfer length method (TLM) test structures which were fabricated using shadow masks to define the

Author Manuscript

This article is protected by copyright. All rights reserved.

contact geometry.[35,36] The contact resistivity was extracted from the *I-V* data obtained from a Keithley 2420 source meter.

The Al / Ca / TiO_2 and Al / TiO_2 contact structures were investigated on polished Si wafers by transmission electron microscopy (TEM). For this purpose, TEM samples were prepared using the focused ion beam (FIB) lift-out method in a Zeiss NVision 40 workstation and thinned down from the Si substrate side (to curtail possible redeposition of species) up to a final thickness of ~80 nm using a final Ga^+ voltage of 2 kV to minimise surface damage and Ga implantation. To reduce Ca oxidation, the samples were quickly transferred from the FIB to a monochromated probe- and image-Cs-corrected FEI Titan Themis microscope, which was operated at 200 kV (air exposure of ~2 mins). Characterisation then involved scanning TEM (STEM) high-angle annular dark-field (HAADF) imaging coupled to either energy-dispersive X-ray spectroscopy (EDX) or electron energy-loss spectroscopy (EELS) using a probe current of 250 or 50 pA, respectively. EEL spectra were recorded in Dual EELS mode using a Gatan GIF Quantum ERS high-energy resolution spectrometer and energy filter with a convergence semi-angle of 20 mrad and a collection semi-angle of 49 mrad. EEL spectra were acquired with an energy resolution of either 400 or 1200 meV depending on whether the monochromator was excited or not.

PRC solar cells (~155 μm thick; ~2×2 cm^2, isolated by a front-side mesa etch) were fabricated on 0.9 Ω.cm n-type float zone silicon wafers. The cells feature a front-side boron diffusion (R_{sheet} ~ 120 Ω/□) on random pyramid texturing, passivated by a SiN_x / Al_2O_3 stack. The planarised rear-sides of the cells were passivated with plasma-enhanced chemical vapour deposited (PECVD) SiN_x. The front contact openings were defined by photolithography and formed by a thermally evaporated Cr / Pd / Ag stack that was later thickened with additional Ag by electroplating. The rear-side contacts were

Author Manuscript

This article is protected by copyright. All rights reserved.

also defined by photolithography prior to the TiO_2 ALD and Ca and Al metal evaporation procedures. The current-voltage (*J-V*) characteristics of the cells were measured using a Sinton Instruments FCT-450 flash tester which was calibrated using a certified reference cell from Franhaufer ISE CalLab.

Supporting Information

Supporting Information is available from the Wiley Online Library or from the author.

Acknowledgements

This work has been supported by the Australian government through the Australian Renewable Energy Agency (ARENA). Work at the University of California, Berkeley was supported by the Bay Area Photovoltaic Consortium (BAPVC). The authors would like to acknowledge Sorin Lazar for his help with monochromated EELS experiments and the Interdisciplinary Centre For Electron Microscopy of EPFL for the use of their microscope.

Received: ((will be filled in by the editorial staff))
Revised: ((will be filled in by the editorial staff))
Published online: ((will be filled in by the editorial staff))

References

[1] C. Battaglia, A. Cuevas, S. De Wolf, *Energy Env. Sci*, **2016**, 9, 1552.

Author Manuscript

This article is protected by copyright. All rights reserved.

[2] Z. C. Holman, A. Descoeudres, L. Barraud, F. Z. Fernandez, J. P. Seif, S. De Wolf, C. Ballif, *IEEE J. Photovolt.*, **2012**, 2, 7.

[3] "NEDO:World's Highest Conversion Efficiency of 26.33% Achieved in a Crystalline Silicon Solar Cell." [Online]. Available: http://www.nedo.go.jp/english/news/AA5en_100109.html. [Accessed: 22-Sep-2016].

[4] M. A. Green, *Sol. Energy Mater. Sol. Cells*, **2015**, 143, 190.

[5] J. Bullock, P. Zheng, Q. Jeangros, M. Tosun, M. Hettick, C. M. Sutter-Fella, Y. Wan, T. Allen, D. Yan, D. Macdonald, S. De Wolf, A. Hessler-Wyser, A. Cuevas, A. Javey, *Adv. Energy Mater.*, **2016**, 6, 1600241.

[6] T. G. Allen, J. Bullock, P. Zheng, B. Vaughan, M. Barr, Y. Wan, C. Samundsett, D. Walter, A. Javey, A. Cuevas, *Prog. Photovolt. Res. Appl.*, **2016**.

[7] A. W. Blakers, A. Wang, A. M. Milne, J. Zhao, M. A. Green, *Appl. Phys. Lett.*, 1989, 55, 1363.

[8] M. A. Green, A. W. Blakers, J. Zhao, A. M. Milne, A. Wang, X. Dai, *IEEE Trans. Electron Devices*, **1990**, 37, 331.

[9] J. Bullock, M. Hettick, J. Geissbuhler, A. J. Ong, T. Allen, C. M. Sutter-Fella, T. Chen, H. Ota, E. W. Schaler, S. De Wolf, C. Ballif, A. Cuevas, A. Javey, *Nat. Energy*, **2016**, 1, 15031.

[10] X. Yang, P. Zheng, Q. Bi, K. Weber, *Sol. Energy Mater. Sol. Cells*, **2016**, 150, 32.

[11] X. Yang, Q. Bi, H. Ali, K. Davis, W. V. Schoenfeld, K. Weber, *Adv. Mater.*, **2016**, 28, 5891.

Author Manuscript

This article is protected by copyright. All rights reserved.

[12] A. F. Thomson, K. R. McIntosh, *Prog. Photovolt. Res. Appl.*, **2012**, 20, 343.

[13] B. Liao, B. Hoex, A. G. Aberle, D. Chi, C. S. Bhatia, *Appl. Phys. Lett.*, **2014**, 104, 253903.

[14] J. Cui, T. Allen, Y. Wan, J. McKeon, C. Samundsett, D. Yan, X. Zhang, Y. Cui, Y. Chen, P. Verlinden, A. Cuevas, *Sol. Energy Mater. Sol. Cells*, **2016**, 158, 115.

[15] A. Richter, S. W. Glunz, F. Werner, J. Schmidt, A. Cuevas, *Phys. Rev. B*, **2012**, 86, 165202.

[16] S. Avasthi, W. E. McClain, G. Man, A. Kahn, J. Schwartz, J. C. Sturm, *Appl. Phys. Lett.*, **2013**, 102, 203901.

[17] K. A. Nagamatsu, S. Avasthi, G. Sahasrabudhe, G. Man, J. Jhaveri, A. H. Berg, J. Schwatz, A. Kahn, S. Wagner, J. C. Sturm, *Appl. Phys. Lett.*, **2015**, 106, 123906.

[18] D. K. Schroder,D. L. Meier, *IEEE Trans. Electron Devices*, **1984**, 31, 637.

[19] R. T. Tung, *Appl. Phys. Rev.*, **2014**, 1, 11304.

[20] R. Sinton, A. Cuevas, *presented at the 16th European Photovoltaics Solar Energy Conference*, Glasgow, Scotland, **2000**.

[21] S. W. Glunz, J. Nekarda, H. Mackel, A. Cuevas, *presented at the 22nd European Photovoltaics Solar Energy Conference and Exhibition*, Milan, Italy, **2007**.

[22] A. F. Carley, P. R. Chalker, J. C. Riviere, M. W. Roberts, *J. Chem. Soc. Faraday Trans. 1: Phys. Chem. Condens. Phases*, **1987**, 83, 351.

Author Manuscript

This article is protected by copyright. All rights reserved.

[23] S. Bartkowski, M. Neumann, E. Z. Fedorenko, S. N. Shamin, V. M. Cherkashenko, S. N. Nemnonov, A. Winiarski, D. C. Rubie, *Phys. Rev. B*, **1997**, 56, 10656.

[24] U. Diebold, *Surf. Sci. Spectra*, **1996**, 4, 227.

[25] Y. Gao, Y. Masuda, Z. Peng, T. Yonezawa, K. Koumoto, *J. Mater. Chem.*, **2003**, 13, 608.

[26] K. Siuzdak, M. Szkoda, M. Sawczak, A. Lisowska-Oleksiak, *New J Chem.*, **2015**, 39, 2741.

[27] Q. Zhang, Y. Li, E. A. Ackerman, M. Gajdardziska-Josifovska, H. Li, *Appl. Catal. Gen.*, **2011**, 400, 195.

[28] S. Tojo, T. Tachikawa, M. Fujitsuka, T. Majima, *J. Phys. Chem. C*, **2008**, 112, 14948.

[29] G. Bertoni, E. Beyers, J. Verbeeck, M. Mertens, P. Cool, E. F. Vansant, G. Van Tendeloo, *Ultramicroscopy*, **2006**, 106, 630.

[30] E. Stoyanov, F. Langenhorst, G. Steinle-Neumann, *Am. Mineral.*, **2007**, 92, 577.

[31] Q. Fu, T. Wagner, *J. Phys. Chem. B*, **2005**, 109, 11697.

[32] B. Demri, M. Hage-Ali, M. Moritz, J. L. Kahn, D. Muster, *Appl. Surf. Sci.*, **1997**, 108, 245.

[33] M. T. Greiner, M. G. Helander, W.-M. Tang, Z.-B. Wang, J. Qiu, Z.-H. Lu, *Nat. Mater.*, **2011**, 11, 76.

[34] A. Agrawal, J. Lin, M. Barth, R. White, B. Zheng, S. Chopra, S. Gupta, K. Wang, J. Gelatos, S. E. Mohney, S. Datta, *Appl. Phys. Lett.*, **2014**, 104, 112101.

[35] R. H. Cox, H. Strack, *Solid-State Electron.*, **1967**, 10, 1213.

Author Manuscript

This article is protected by copyright. All rights reserved.

[36] D. L. Meier, D. K. Schroder, *IEEE Trans. Electron Devices*, **1984**, 31, 647.

Author Manuscript

Figure 1. (Excess carrier lifetime of TiO_2 passivated 1 Ω.cm n-type silicon as a function of injection level measured using the photoconductance decay technique.)

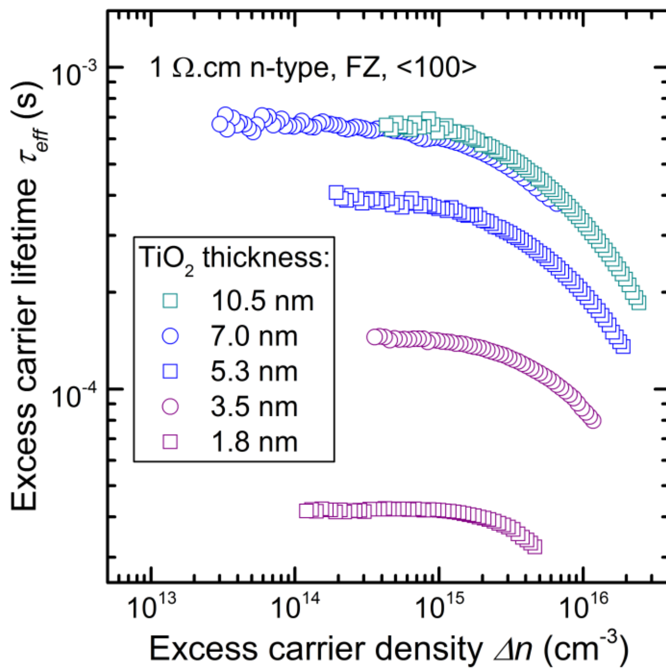

Figure 2. (a) *J-V* measurements of contact resistance test structures showing rectifying (Schottky) behavior of the Al / n-type Si and Al / TiO_x / n-type Si contacts, and the Ohmic behavior of the Ca / n-type Si contact; and b) contact resistivity extracted from TLM test structures for Ca / Si and Ca / TiO_x / Si contacts.)

This article is protected by copyright. All rights reserved.

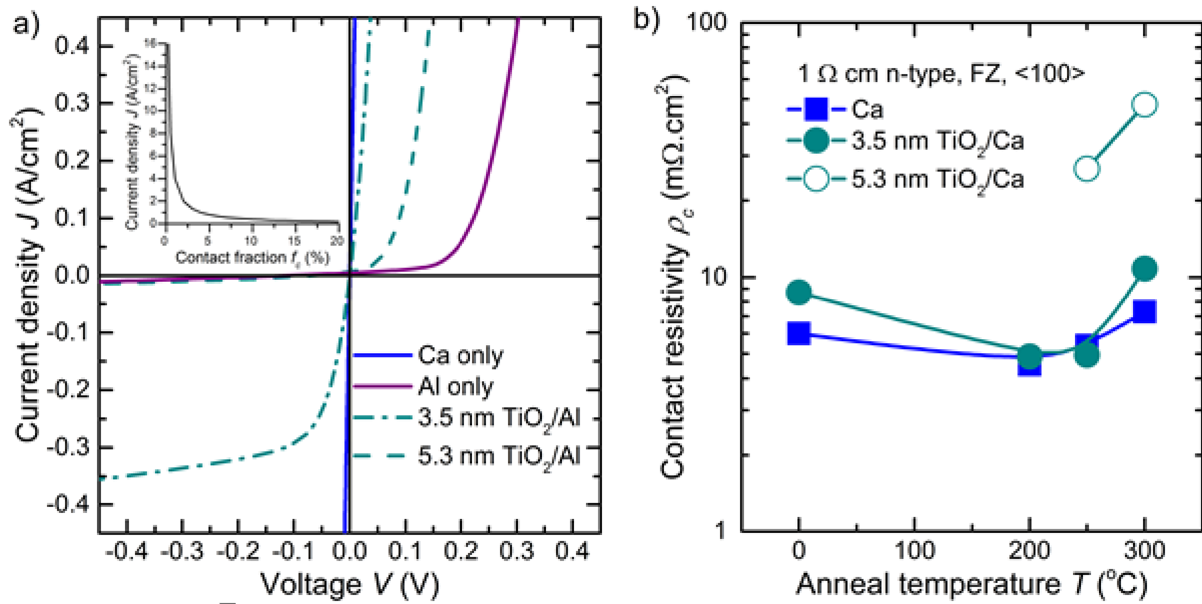

Author Manuscript

Figure 3. (a) Schematic of the passivated, partial rear contact (commonly known as 'PERC') solar cell structure fabricated in this study; b) one sun *J*-*V* curves of the PRC solar cells fabricated with and without a passivating TiO_x interlayer. Note that the TiO_x cell has a higher rear contact fraction (f_c = 6.25%) compared to the reference cell without the TiO_x (f_c = 1.26%).

This article is protected by copyright. All rights reserved.

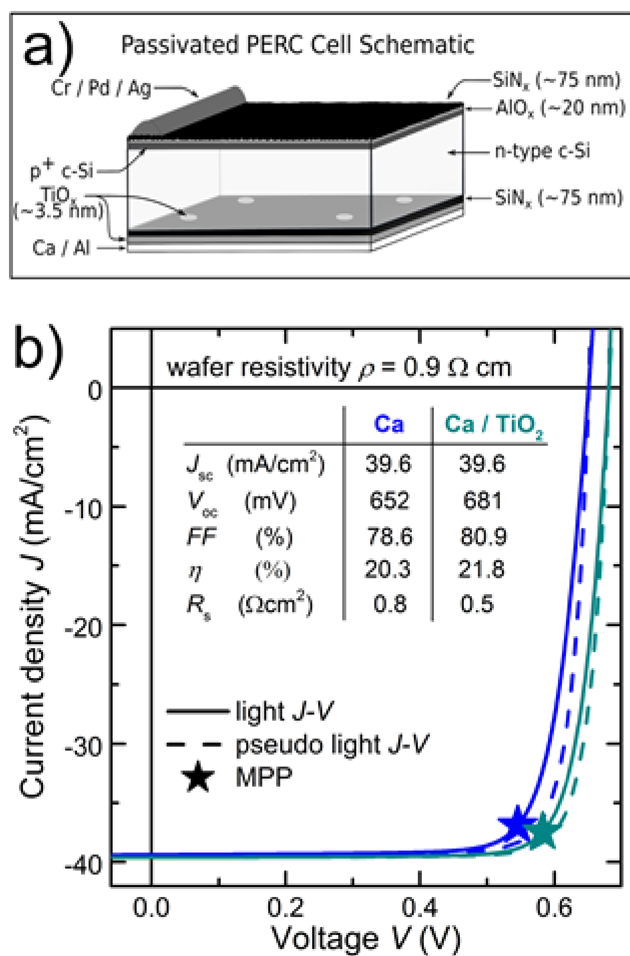

Figure 4. (XPS of the ALD titania prior to metalisation indicating a near stoichiometric atomic ratio of TiO_x, $x \approx 2$. (Inset: the O1s spectra).)

Author

This article is protected by copyright. All rights reserved.

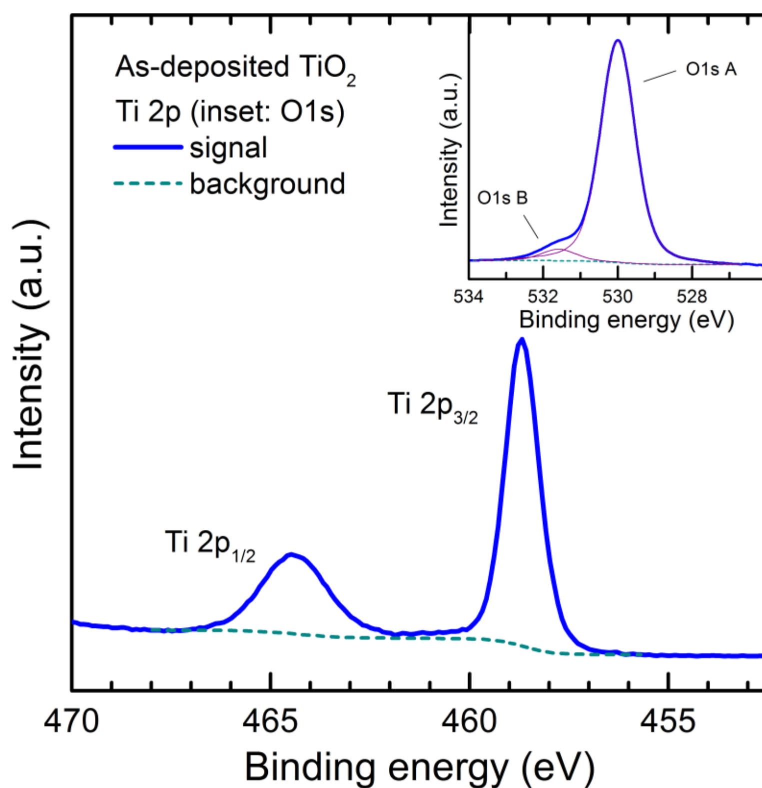

Author Ma

Figure 5. (STEM HAADF imaging with EDX elemental mapping (a) of the Al / Ca / TiO_x / Si contact structure. High resolution STEM (b) with EELS (c) of the same Al / Ca / TiO_x / Si contact. The EDX and EELS both show the Ca intermixing with the TiO_x layer. Higher energy resolution EELS taken from both the Al / TiO_x / Si and Ca / TiO_x / Si contacts are shown in (d). Analysis of the high resolution EEL spectra indicate a reduction in the titania after the application of the contact metals.).

This article is protected by copyright. All rights reserved.

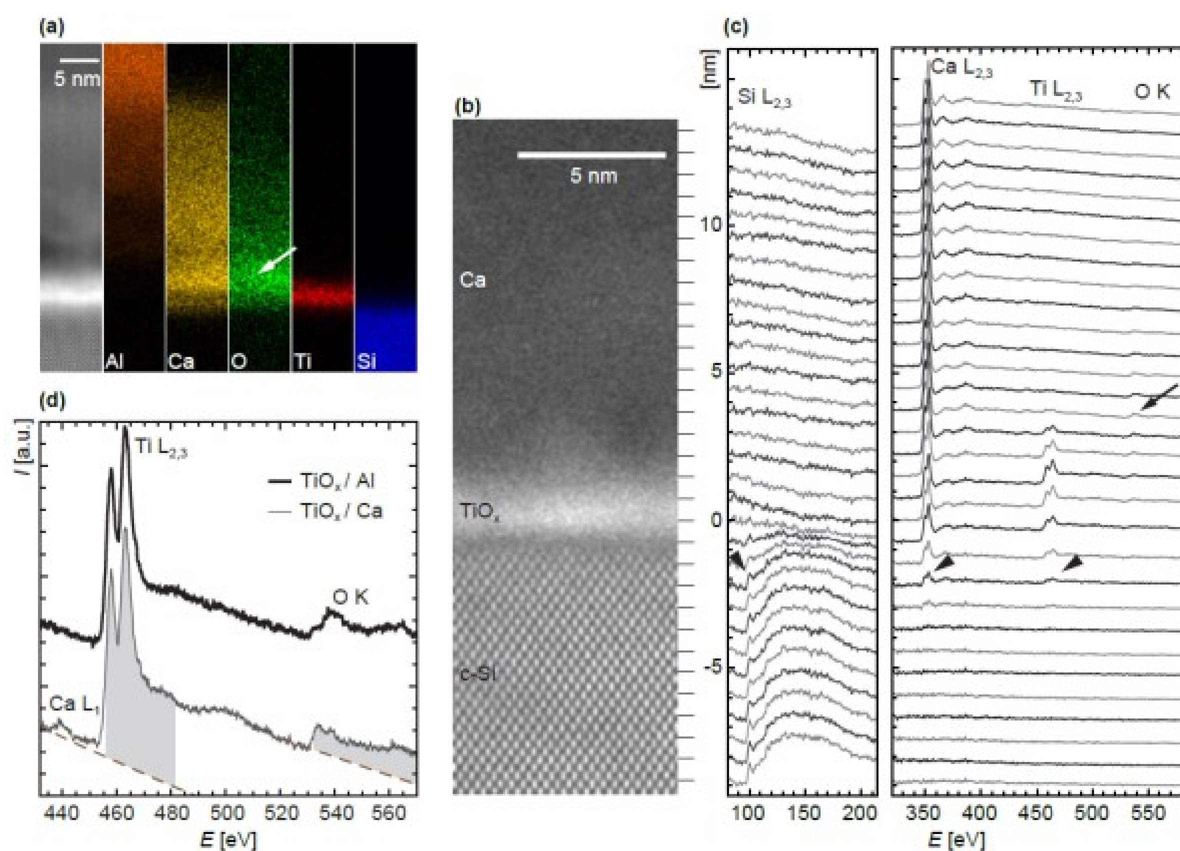

Table of Contents:

A novel passivated contact on crystalline silicon comprised of calcium and reduced titania is shown to result in a reduction in contact resisitivity by up to two orders of magnitude compared to other titania-based contacts to crystalline silicon. This has enabled the fabrication of a first-of-its-kind passivated n-type c-Si PERC cell with an efficiency of 21.8%.

Authors: Thomas G. Allen, James Bullock, Quentin Jeangros, Christian Samundsett, Yimao Wan, Jie Cui, Aïcha Hessler-Wyser, Stefaan De Wolf, Ali Javey and Andres Cuevas*

Title: A Low Resistance Calcium / Reduced Titania Passivating Contact for High Efficiency Crystalline Silicon Solar Cells

Author Manuscript

This article is protected by copyright. All rights reserved.

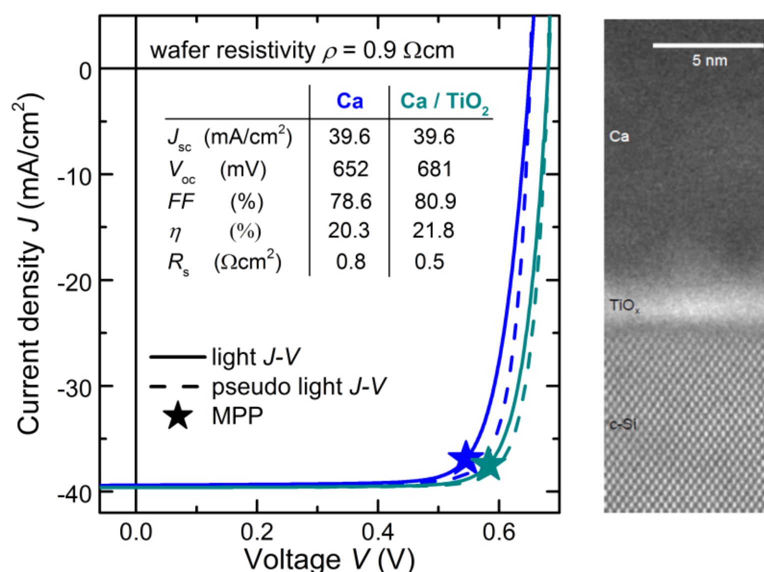

Author Manuscript

Supporting Information

Making the Case for Partial Rear Contacts

Authors: Thomas G. Allen, James Bullock, Quentin Jeangros, Christian Samundsett, Yimao Wan, Jie Cui, Aïcha Hessler-Wyser, Stefaan De Wolf, Ali Javey and Andres Cuevas*

The application of a passivating interlayer to the rear side of a PRC cell design can not only result in higher device performance but can also free up constraints on cell fabrication with regards to wafer resistivity. In **Figure S1** the n-type PRC cell structure reported in Ref. [1] is modelled in Quokka2 using parameters listed in **Table S1**, following previously reported empirical data.[1,2] In the Figure, the modelled device efficiency is reported as a function of both the wafer resistivity and rear contact recombination current parameter J_{0c}. The modelling predicts, as was previously demonstrated by the

This article is protected by copyright. All rights reserved.

authors,[1] a monotonic increase in efficiency with increasing doping (in the range of resistivities modelled) for devices with poorly passivated rear contacts, representative of devices with directly metallised rear contacts. The high sensitivity of this directly metallised device architecture on recombination at the rear contact is due to the fact that as the base doping increases, the minority carrier concentration decreases, and so too the recombination rate. This decrease in the recombination rate also has an impact on internal series resistance due to higher carrier concentrations, and so higher conductivity in the silicon wafer.[1]

Figure S1. (Modelling of cell designs reported in Ref. [1] (Figure S1a) and this work (Figure S1b) as a function of wafer resistivity and rear contact recombination parameter J_{0c}. The three sets of curves in each Figure are representative of the three cases explored: an infinite lifetime in the silicon bulk material (solid curves); the introduction of a defect that limits the bulk lifetime (dashed curves); and an infinite bulk lifetime with a front side selective emitter (dot-dash curves). The stars represent the empirical results from the *J-V* curves in Figure 3b).)

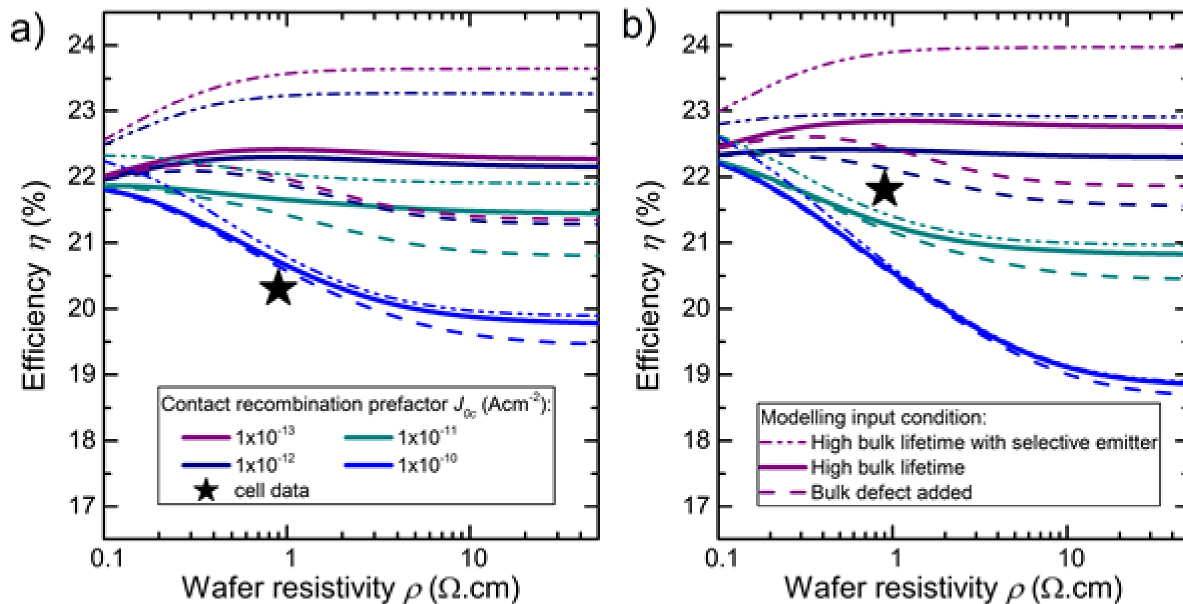

This article is protected by copyright. All rights reserved.

Table S1. (Modelling input parameters.)

Input parameter	
Wafer type/thickness	n-type / 155 µm
Front J_0	72 or 15 fA.cm^{-2}
Front ρ_c	1x10^{-6} Ω.cm^2
J_{gen}	40 mA.cm^{-2}
Bulk τ	Infinite or bulk limiting defect
Rear ρ_c	5x10^{-3} Ω.cm^2
Rear f_c	1.26% or 6.25%
Rear J_0 (non-contacted)	3 fA.cm^{-2}
R_s	0.3 Ω.cm^2
R_{sh}	10000 Ω.cm^2

Author Manuscript

This article is protected by copyright. All rights reserved.

Author Manuscript

This trend changes when passivated contacts are introduced. Reducing the recombination losses at the rear point contacts (decreasing J_{0c}) results in a flattening of the curve, until Auger recombination becomes a dominant loss mechanism as the wafer resistivity approaches 0.1 Ω.cm. Comparing Figures S1a) and S1b), the modelling shows that by increasing the contact fraction f_c, the effect of J_{0c} becomes more pronounced as the wafer resistivity increases. This leads to a higher efficiency potential in the lowest J_{0c} case (as series resistance losses are reduced) and a lower efficiency potential for the highest J_{0c} case (as contact recombination losses dominate), seen in the wider divergence of the modelled data in Figure S1b) compared to Figure S1a) at high resistivities. At lower resistivities the modelling shows that all J_{0c} conditions for the larger f_c case result in a higher efficiency compared to the lower f_c case: the recombination at the contacts is again being mitigated by the higher wafer doping, even when comparing the data for the highest J_{0c} in Figure S1b) with the lowest in Figure S1a), despite the significantly larger area of the recombination active regions.

It is worth noting that the addition of a passivating interlayer between the undiffused contact region and the overlying low work function metal in the PRC cell architecture modelled here serves much the same function as the addition of localised dopant diffusions underneath the metal electrode in the PERL cell *vs.* the PERC cell. In the PERL cell design, constraints on base doping are lifted as the heavily doped sub-surface contact region reduces the SRH recombination rate at the silicon-metal interface at the expense of introducing additional Auger recombination losses. One point of difference regarding the calcium based PRC devices modelled here is that, in the case of the PERL *vs.* PERC cell structures the heavy doping under the metal contacts also serves to free up the critical dependence of contact resistivity with base doping, a condition that limited the fabrication of the

This article is protected by copyright. All rights reserved.

PERC cells to wafer resistivities less than 0.5 Ω.cm.[3] As the low work function enabled contacts in this contribution, as in Refs. [1] and [2], operate via thermionic emission (and not thermionic field emission through a narrowed barrier width, as is the case for diffused and alloyed contacts) this dependence on ρ_c with wafer resistivity is already relaxed.

Notably, as recently reported by Steinkemper *et al.*,[4] the PERL cell architecture (and so too the passivated PRC cell presented here) is sensitive in the efficiency response to wafer resistivity with respect to bulk lifetime, unlike cell architectures that feature full area rear contacts, like the SHJ and TOPCon cells.[5] This is shown in Figure S1, where a midgap bulk defect is introduced. The defect parameters are such that the lifetime of a 1 Ω.cm n-type wafer is limited to 1 ms at an injection level of Δn = 1×10^{15} cm^{-3} and, given that the capture cross section ratio has been fixed to unity, little injection dependence in the minority carrier lifetime is introduced, which is known to result in lower fill factors at the device level.[6] This same defect is applied to each wafer resistivity / J_{0c} combination, resulting in the dotted lines in Figure S1.

The decrease in efficiency with increasing wafer resistivity, as in the cells with poorly passivated contacts, and the cells with well passivated contacts but lower bulk lifetime, can be largely attributed to an increase in internal series resistance losses. This is due to the reliance of the PERC and PERL architectures to transfer carriers laterally, as well as vertically, to the rear contacts through the bulk of the device, and not through diffused regions (as in the PERT - passivated emitter, rear totally diffused - cell) or conductive overlayers (as in SHJ cells). Such lateral conductivity issues are of course eliminated with respect to current flows in full rear area contact schemes, as emphasised in Ref. [4] and [5]. This effect could also be mitigated in PERC cell designs if the contact pitch and diameter could be considerably reduced, such that the rear current flows become quasi-1D.[3,7]

Author Manuscript

This article is protected by copyright. All rights reserved.

Author Manuscript

Nevertheless, this dependence of the efficiency on bulk lifetime offers substantial challenges to the manufacturing conditions of cells with partial rear contacts, where sensitivity to metallic surface impurities, even in n-type wafers, is a concern when high temperature processes are performed.[8,9] It follows that eliminating high temperature processes, like thermal dopant diffusions, and adopting passivated heterocontacts, could increase the yield across a wider range of wafer dopant densities throughout the silicon ingot for solar cells manufactured with dopant-free, partial rear contacts.

Finally, the same devices have been modelled with a reduction in front side recombination, using the data on the selective emitter structure reported in Ref. [5]. As can be seen in Figures S1a) and S1b), the introduction of a selective emitter to the front side of the cell makes a significant impact on device performance only when the recombination at the rear contacts is significantly suppressed, or when the wafer resistivity is very low. Note that the modelling of the devices with the reduced front recombination has been conducted without the introduction of a bulk defect. Adding the bulk defect creates an identical trend as for the cells modelled with the higher front side J_0 and so is not shown. It is also noteworthy that increasing the generation current from 40 mA/cm^2 to 42.1 mA/cm^2, as reported in Ref. [5], lifts the maximum efficiency of the cells modelled with the best contact passivation and largest contact fraction to over 25%, identifying one limitation of using Ca as the rear metal rather than more highly reflective metals like Ag or even Al.[1] Furthermore, as the modelling here fixes the contact fraction f_c and varies other inputs, the cells are not necessarily optimised for the rear contact area; the optimum f_c would indeed change as recombination, resistivity and bulk lifetime change. Nevertheless, the modelling indicates numerous potential advantages of the passivated PERC cell architecture: a significantly higher efficiency potential for a wider range of

This article is protected by copyright. All rights reserved.

wafer resistivities, with a potential for enhanced manufacturability and yield, compared to PERC cell structure of Ref. [10].

Author Manuscript

References:

[1] T. G. Allen, J. Bullock, P. Zheng, B. Vaughan, M. Barr, Y. Wan, C. Samundsett, D. Walter, A. Javey, A. Cuevas, *Prog. Photovolt. Res. Appl.*, **2016**.

[2] J. Bullock, P. Zheng, Q. Jeangros, M. Tosun, M. Hettick, C. M. Sutter-Fella, Y. Wan, T. Allen, D. Yan, D. Macdonald, S. De Wolf, A. Hessler-Wyser, A. Cuevas, A. Javey, *Adv. Energy Mater.*, **2016**, 6, 1600241.

[3] M. A. Green, A. W. Blakers, J. Zhao, A. M. Milne, A. Wang, X. Dai, *IEEE Trans. Electron Devices*, **1990**, 37, 331.

[4] H. Steinkemper, M. Hermle, S. W. Glunz, *Prog. Photovolt. Res. Appl.*, **2016**, 24, 1319.

[5] S. W. Glunz, F. Feldmann, A. Richter, M. Bivour, C. Reichel, H. Steinkemper, J. Benick, M. Hermle, *presented at the 31st European Photovoltaic Solar Energy Conference and Exhibition,* Hamburg, Germany, **2015**.

[6] D. Macdonald, A. Cuevas, *Prog. Photovolt. Res. Appl.*, **2000**, 8, 363.

[7] A. Cuevas, *IEEE J. Photovolt.*, **2012**, 2, 485.

This article is protected by copyright. All rights reserved.

[8] D. MacDonald, A. Cuevas, K. McIntosh, L. Barbosa, D. De Ceuster, *presented at the 20th European Photovoltaic Solar Energy Conference*, Barcelona, Spain, 2005.

[9] J. Schmidt, B. Lim, D. Walter, K. Bothe, S. Gatz, T. Dullweber, P. P. Altermatt, *IEEE J. Photovolt.*, **2013**, 3, 114.

[10] A. W. Blakers, A. Wang, A. M. Milne, J. Zhao, M. A. Green, *Appl. Phys. Lett.*, **1989**, 55, 1363.

Author Manuscript

This article is protected by copyright. All rights reserved.